Energy Equip. Sys. / Vol. 9/No. 3/Sep. 2021/ 209-227

ENERGY EQUIPSYS

Energy Equipment and Systems

http://energyequipsys.ut.ac.ir
www.energyequipsys.com

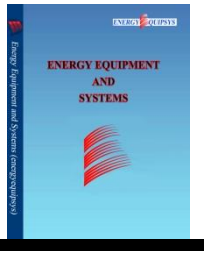

Heat transfer enhancement in solar air heater with turbulent natural convection by two flapping elastic winglets

Authors

Seyyed Abdolreza Gandjalikhan Nassab [a*]
Maryam Moein Addini [a]

[a] Department of Mechanical Engineering, School of Engineering, Shahid Bahonar University of Kerman, Kerman, Iran

ABSTRACT

The positive effect of self-sustained passive oscillations of two flexible vortex generators (VGs) in the naturally air flow of a solar air heater (SAH) is examined in this paper. Two VGs are attached on opposite walls of 2-D channel of the heater, where the turbulent air flows because of the buoyancy effect. The set of continuity, momentum and energy equations for free convection flow and also the equation of motion for elastic solid structure considering a two-way strongly-coupled fluid-solid interaction (FSI) are solved in transient condition by the finite element method (FEM). Numerical result shows higher performance for SAH with two VGs in comparison with a single winglet and also with clean SAH. Although, the airflow rate decreases about 16% in SAH with two VGs because of the blockage effect of winglets, but 35% improvement in bulk temperature increase along the SAH is seen in comparison to the single VG solar heater. The applied numerical simulation has been validated against experimental and theoretical results of literature and good agreement was found.

Article history:

Received : 4 November 2020
Accepted : 29 December 2020

Keywords: Natural SAH, Turbulent Flow, Multiple VG, Transient

1. Introduction

Today, the energy deficiency forces governments to avoid fossil energy consumption and use renewable energies. For this purpose, there are several ways to achieve this goal, from waste energy harvesting, energy management via intelligent supervisory predictive control as well as using energy sources such as geothermal, solar, and wind energy. Even with the current rate of energy consumption, there is a considerable gap between total demand and providing renewable energy. At the moment, solar energy has been widely considered due to its availability and also effectiveness in the emission of pollutants. In a general form, solar heaters as heat exchangers are used for converting solar radiation into enthalpy of a carrier fluid which may be employed as a heat source in many engineering systems. They are very popular due to their special features such as simplicity and economically affordable expenses to be built or purchased.

* Corresponding author: S.Abdolreza Gandjalikhan Nassab
Department of Mechanical Engineering, School of Engineering, Shahid Bahonar University of Kerman, Kerman, Iran
Email: ganj110@uk.ac.ir

The natural convection flow solar air heaters are simple devices that convert solar irradiation into gas enthalpy at moderate temperatures for employing in many engineering applications, such as heating and cooling spaces and drying agricultural products. The most common design of natural convection plane SAH consists of a uniform rectangular cross-sectional duct throughout its length with a glass cover at the front and a black absorber plate at the back. The transmitted solar incident radiation across the glass sheet is absorbed and then transferred into airflow by convection heat transfer (Fig. 1). But, the rate of heat transfer between the absorber and air is poor because of the very low thermal conductivity and velocity of the working gas. One major challenge that researchers have focused their investigations is on the design aspect that improves the thermal performance and enhances the convection heat transfer between the airflow and heated surface by different techniques. Several numerical and experimental scientific works have been published just to attack this issue and propose a new solution to enhance SAH's thermal performance. The ideas include extending surface area [1], bell-shaped for the inlet section [2], convex and concave channels for different curvature radii [3], serpentine wavy wire-mesh packed bed [4], internal multiple-fin array in the direction of airflow [5] as well as a new geometry of arched absorber [6]. The concept of extruded surfaces such as baffle [7], straight [8], and multiple V-shaped [9] or inclined ribs [10] for SAH also has been considered by some investigations. Enhancement of thermal performance through the employment of impinging jet generated by corrugated wavy plate for configuration of double pass SAH was reported by Singh et al.[11]. It was shown that the applied technique causes a considerable increase in the value of efficiency by breaking the thermal boundary layer and mixing enhancement.

To improve the thermal efficiency of solar heaters, the author recently investigated the effect of gas radiation on the thermal behavior of forced convection flow when a radiating working gas inside a closed cycle is used instead of air [12]. In that study, the set of governing equations including the conservations of momentum and energy for the gas flow and conduction equation for the solid parts of a single pass solar heater were solved simultaneously, while the radiation transfer equation was also solved for radiation computation. It was revealed that using high optically thick fluid flow can improve the performance of solar heaters by about 100%. The same technique was also examined by the author in double-flow solar gas heaters [13]. It was found that there is an optimum value of the gas optical thickness for having the best performance for double flow solar heaters.

The rate of convection heat transfer can also be improved by creating disturbance to the flow of air inside the channel. Many types of vortex generators for heat transfer enhancement have been investigated up to now. In general, stationary VGs and flapping VGs are the two main categories for the generation of vortices. For various stationery designs, transverse or longitudinal vortices can be generated in convection flow to be enhanced [14, 15].

Instead of stationary VGs, a flapping vortex generator made of elastic material can be placed in the existing duct directly for more heat transfer. It is clear that the frequency of VG is much affected by the value of its Young modulus of elasticity. Flapping vortex generators oscillate in the channel to create vortices for mixing and breaking the resistance of the thermal boundary layer. To fulfill the flapping vortex generators, two ways exist; the active method with external power and the passive method with fluid-structure interaction. It is evident that an additional power supply system is required for active VGs to drive structure oscillation, limiting their application range. In recent years, fluid-structure interaction (FSI) has been a topic of interest in many engineering fields [16, 17]. This disturbance creates turbulence in the airflow and hence heat transfer enhancement in convective flow.

The elastic structure mounted on the heat exchanger fins can enhance the heat transfer significantly, even mounting multiple elastic structures on the fin has been discussed in the literature [18, 19].

Flow-induced deformation of a flexible thin structure as the manifestation of heat transfer enhancement in laminar convection heated channel flow was numerically studied by Soti et al. [20]. The in-house fluid-structure interaction

(FSI) solver with convective heat transfer was based on a sharp-interface immersed boundary method (IBM) An elastic thin plate attached on the lee side of a rigid cylinder had the role of vortex generator. The positive effects of flow vortices on enhancing convection coefficient along the heated wall were thoroughly explored.

A three-dimensional numerical analysis of the convective heat transfer and mixing performances of pipe flows was done by Ali et al.[21]. All numerical simulations based on fluid-solid interactions were carried out by the ANSYS Fluent CFD solver. Both flexible and rigid vortex generators were considered in the simulation. Numerical results revealed about 97% and 118% increase in the value of average Nusselt number for rigid and flexible winglets, respectively. In a recent study, Zheng et al. [22] analyzed the flapping vortex generator mounted on a heat sink fin for airside heat transfer enhancement by numerical method. Three elastic agitators and one rigid agitator were investigated, separately, under two velocities of convection flow, while the results are compared with those of a clean channel. It was found that the elastic agitator enhances the channel heat transfer significantly, especially when the winglet oscillates with high velocity. There are several similar studies on this subject, but the literature review shows that this technique in enhancing convection heat transfer has not been examined on naturally flow SAHs, yet. To fill this gap, the author tried for investigating the effect of oscillating elastic VGs on transient thermohydrodynamic characteristics of turbulent natural airflow in SAHs using one and multiple flapping VGs. In the numerical simulation, the time-dependent air velocity is determined by balancing the buoyancy head resulting from thermally induced density differences and the friction head due to wall shear stresses through the governing equations. Toward this end, the set of conservation equations including the mass, momentum and energy for turbulent natural convection flow was solved numerically and simultaneously by progressing in time from the initial state, while all parts are at ambient temperature and air is stagnant. To describe the oscillation of the two-dimensional elastic flapping vortex generator, the equations of motion along with a two-way strongly-coupled fluid-solid interaction along with flow equations have been solved, simultaneously progressing in time. It is worth mentioning that in vortex generation, the Strouhal number ($fL_{VG}/\bar{V}$) is a dimensionless parameter describing the relationship among vortex shedding frequency, characteristic length, and velocity. Also, there is a relation between the winglet frequency and Strouhal number for having more convection enhancement and flow vortices with higher rates. But the frequency of passive flapping winglets depends on the VG dimension, its Young modulus and flow condition, and is not as an input data in the present simulation. All computations have been performed by the finite volume method using the COMSOL multi-physics and the results were presented in the forms of velocity and temperature contours and the variations of dependent variables with time. Comparison was conducted between the present numerical results and experimental data for validating the applied numerical model.

Nomenclature

b	thickness of the air layer (m)
c_p	specific heat (kJ/kg K)
E	module of elasticity (Pa)
f	Frequency (1/s)
h	convection coefficient (W/m^2K)
k	thermal conductivity ($Wm^{-1}K^{-1}$)
L	length of heater (m)
n	normal to the surface
$\dot{m}$	mass flow rate (kg/s)
Pr	Prandtl number
q	heat flux (W/m^2)
Re	Reynolds number
Ra	Rayleigh umber
t	time (s)
T	temperature (K)
T_{in}	inlet temperature (K)
U	time average flow velocity (m/s)
U_s	displacement vector of VG (m)
(x, y)	Vertical and horizontal coordinates (m)

Greek symbols

α	thermal diffusivity (m^2/s)

β	volumetric thermal expansion(1/K)
δ	attacked angle (degree)
ν	Poisson ratio
σ	solid stress field (Pa)
Γ	fluid stress field (Pa)
λ	Lame's first parameter (Pa)
κ	turbulence kinetic energy(m^2/s^2)
μ_s	Lame's second parameter (Pa)
μ	viscosity (kg/ms)
ρ	density (kg/m^3)
Δ	winglet thickness (mm)

subscript

abs	absorber
conv	convection
i, j	indices in tensor notation
m	mean bulk
rad	radiation
t	turbulence (total)
s	solid
1,2	first and second VG

superscript

'	fluctuation
-	time average

2. Description of problem

A schematic of the SAH understudy with its geometrical parameters is depicted in Fig.1. The length of SAH is equal to L and the air gap is denoted by b. Two identical oscillating winglets attached to the boundary surfaces with the same attacked angle have the role of vortex generator. The transmitted solar radiation from the glass cover is absorbed by the absorber and then by the air adjacent to the heated wall with convection heat transfer. Consequently, by natural convection, air enters from the inlet section in x-direction, and buoyancy force pushes it towards the outlet at the front because of the density gradient. The absorber surface is under a constant solar heat flux, while the convection boundary condition is employed on the opposite wall.

The behavior of buoyant airflow strictly depends on the flow regime within the SAH. In these cases, Rayleigh number can be used as a criterion to assess the flow regime which is defined as:

$$Ra = \frac{g\rho\beta\Delta T L^3}{\mu\alpha} \tag{1}$$

In Eq. (1), ΔT is the temperature difference between the absorber and air and L is the length of the solar chimney. According to the reported critical values in literature, the flow regime changes from laminar to turbulent for Rayleigh number greater than 10^9, as it is in the case [23].

3. Mathematical formulation

For two-dimensional unsteady free convection turbulent incompressible flow with employing the Boussinesq approximation, the mass, momentum, and energy conservation equations can be written as follows:

$$\frac{\partial}{\partial x_i}(\rho U_i) = 0 \tag{2}$$

$$U_j \frac{\partial(\rho U_i)}{\partial x_j} = -\frac{\partial p}{\partial x_i} + \frac{\partial}{\partial x_j}(\mu \frac{\partial U_i}{\partial x_j} - \rho \overline{u_i u_j}) - \rho\beta g_i (T - T_{ref}) + F_i \tag{3}$$

$$U_j \frac{\partial(\rho T)}{\partial x_j} = \frac{\partial}{\partial x_j}(\frac{\mu}{\Pr}\frac{\partial T}{\partial x_j} - \rho \overline{T' u_j}) \tag{4}$$

where, $\overline{u_i u_j}$ and $\overline{T u_j}$ are the Reynolds stresses and turbulent heat fluxes which should be modeled. Also, F_i in Eq. (3) is the momentum forcing term that enforced the no-slip condition on the winglet. Based on the applied $\kappa-\varepsilon$ turbulence model in the present study, the Reynolds stresses and turbulent heat flux were computed with the following equations [23].

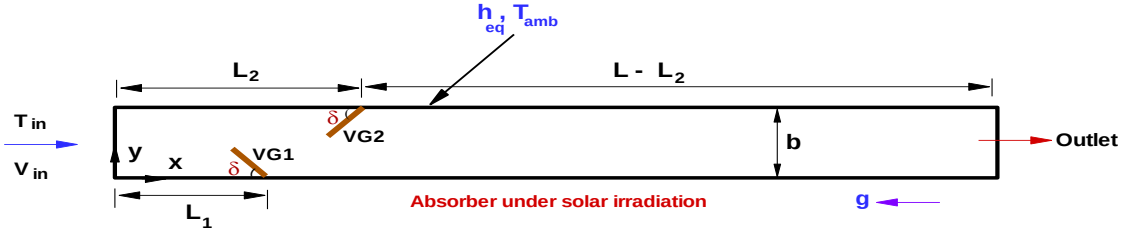

Fig. 1. Schematic of problem

$$\overline{u_i u_j} = -\nu_t\left(\frac{\partial U_i}{\partial x_j} + \frac{\partial U_j}{\partial x_i}\right) + \frac{2}{3}\kappa\delta_{ij} \tag{5}$$

$$\overline{\theta' u_j} = -\frac{\nu_t}{\mathrm{Pr}_t}\frac{\partial T}{\partial x_j} \tag{6}$$

$$\nu_t = C_\mu \frac{\kappa^2}{\varepsilon} \tag{7}$$

The turbulent kinetic energy κ and its dissipation rate ε were calculated by the following coupled partial differential equations:

$$U_j\frac{\partial \kappa}{\partial x_j} = \frac{\partial}{\partial x_j}\left[\left(\nu + \frac{\nu_T}{\sigma_k}\right)\frac{\partial \kappa}{\partial x_j}\right] + (P_k + G_k) - \varepsilon \tag{8}$$

$$U_j\frac{\partial \varepsilon}{\partial x_j} = \frac{\partial}{\partial x_j}\left[\left(\nu + \frac{\nu_T}{\sigma_\varepsilon}\right)\frac{\partial \varepsilon}{\partial x_j}\right] + \frac{\varepsilon}{\kappa}\left[C_{\varepsilon_1}(P_k + G_k) - C_{\varepsilon_2}\varepsilon\right] \tag{9}$$

In Eqs. (8) and (9), G_b and G_k represent the turbulence kinetic energy generation due to buoyancy and velocity gradient, respectively. The values of these parameters and also other constants in turbulent governing equations were given in Refs. [23, 24].

The equation of motion for computing the oscillation of 2-D flapping VG under the convection flow can be driven as [22]:

$$(\lambda + \mu_s)\frac{\partial}{\partial x_i}\left(\frac{\partial U_{sj}}{\partial x_j}\right) + \mu_s\frac{\partial}{\partial x_j}\left(\frac{\partial U_{si}}{\partial x_j}\right) = \rho_s \ddot{U}_{si} \tag{10}$$

where U_{si} is the displacement vector of the elastic sheet. More details about the equation govern to the displacement of elastic winglet were given in the paper by Zheng et al. [22].

4. Boundary condition

The set of governing equations was solved simultaneously in transient conditions by marching in time. Also, the turbulent $\kappa-\varepsilon$ model was used to describe the turbulent heat fluxes and Reynolds stresses. In numerical solution, the following initial and boundary conditions were imposed:

- At t=0, the air is stagnant at ambient temperature (293 K).
- The air pressure at the inlet and outlet sections is equal to ambient pressure (zero gauge pressure).
- The convection boundary condition with its equivalent convection coefficient on the glass surface was employed. The convective and radiative parts of the equivalent coefficient of heat transfer were calculated based on the following expressions [25]:

$$h_{conv} = 5.7 + 3.8V_{wind} \tag{11}$$

$$h_{rad} = \sigma\varepsilon_g\left(\frac{T_w^4 - T_{sky}^4}{T_w - T_{amb}}\right) \tag{12}$$

where

$$T_{sky} = 0.0522T_{amb}^4 \tag{13}$$

- On the absorber surface, constant heat flux was assigned.
- The continuous boundary conditions of the velocity and stress fields of VG yield to the following criteria.

$$U_i = \dot{U}_{si} \tag{14}$$

$$\sigma_{ij}n_j = \Gamma_{ij}n_j \tag{15}$$

where n_j is the local normal pointing outward from the surface. In Eqs. (14) and (15), the stress fields inside the solid and fluid are given by:

$$\sigma_{ij} = \mu_s[(U_{si,j} + U_{sj,i})] + \frac{\lambda}{2}tr(U_{si,j} + U_{sj,i}) \tag{16}$$

$$\Gamma_{ij} = -p\delta_{ij} + \mu[U_{i,j} + U_{j,i}] - \frac{2}{3}\mu U_{i,i}\delta_{ij} \tag{17}$$

Because of the moving VG, the computational region for the fluid flow is considered as the deforming domain and the flow equations were solved by moving mesh technique designed in the COMSOL multiphysics. In velocity and temperature computations, all thermophysical properties of working gas were considered temperature-independent evaluated at average fluid bulk temperature, except density which was determined by the Boussinesq approximation. The finite element method (FEM) was used for discretization of the governing equations. The unstructured triangular grid generation method was used for the 2D geometry of SAH as shown in Fig. 2, such that near the walls and around the vibrating winglet, mesh was refined to precisely capture the high gradient of dependent variables. The optimum number of nodes in simulation of SAH with two VGs is 13240 with average element's quality of 0.89. This grid size was obtained by the grid independent study, such that 10% increase in the number of grids yields to less than 1% variation in the computed value of the

average temperature on absorber surface as a sensitive dependent variable to the grid size. The related results are tabulated in Table. 2. Besides, the convergence criteria were considered equal to 5×10^{-4} for temperature and 10^{-4} for velocity computations for the converged solution at each time step. The final time is determined as the system reaches to its periodic behavior.

5. Validation

At first, for validating the applied mathematical model for natural convection simulation, the present numerical results were compared with the experimental data of the literature [26]. A large vertical channel with one-sided heated wall in which the buoyant air flows because of the density gradient was studied in this test case. The chimney under experimental study in Ref. [26] was a rectangular-shaped channel whose height is 8 m and the width and depth is 0.5 m (Fig. 3). In the numerical simulation, a two-dimensional model was assigned which is dimensionally identical to the experimental set-up having a 2-D vertical channel of height 8m and width 0.5 m. One wall of the channel is maintained at constant temperature 423 K and the other sidewall is adiabatic. All boundary walls are gray surfaces with an emissivity of 0.9. Also, the ambient air temperature is equal to 293 K. The value of the Rayleigh number for this test case is equal to 5×10^{12} correspondence to the turbulent natural flow. In Fig. 3, the velocity and temperature variations across the channel width at y=7.8 m have been compared with the experimental data of Ref. [26]. As seen, good consistencies exist between the predicted velocity and temperature distributions and experiments.

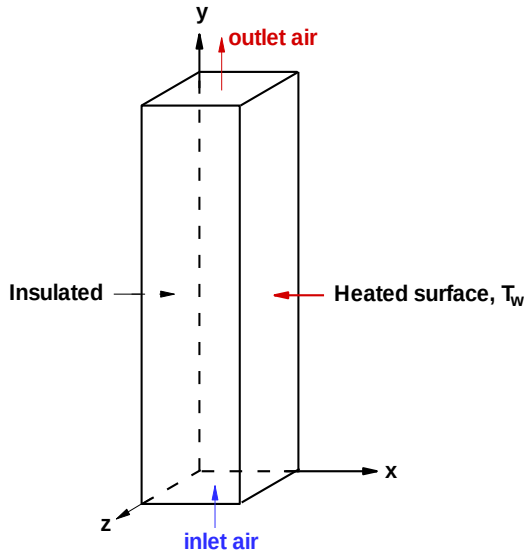

a) Schematic of the experimental set up [26]

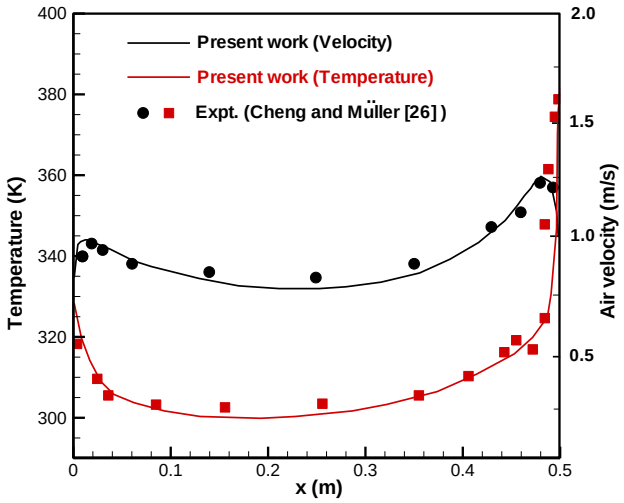

b) Comparison with experiment

Fig. 3: Velocity and temperature distributions at y=7.8 m, comparison with experiment [26].

Table 2. The average temperature on the absorber surface at different grid sizes

Number of grids	8650	9980	11840	13240	14600
$\bar{T}_{abs}$ **(K)**	398	412	424	431	435

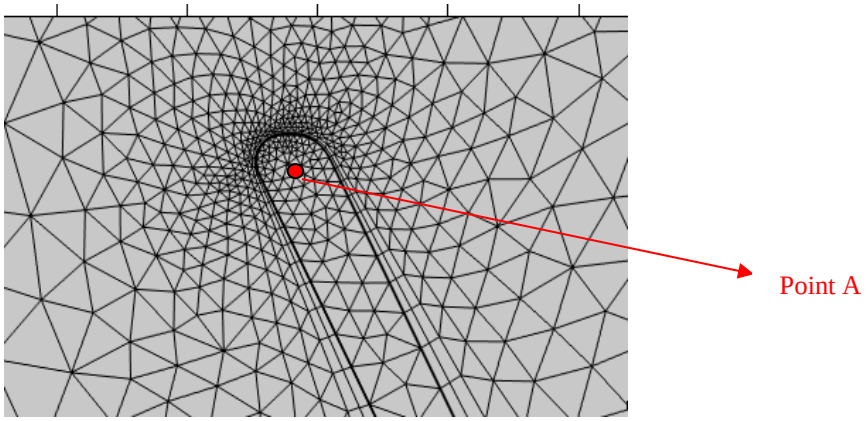

Fig. 2. High enlarged discretized domain

In another test case about enhancing heat transfer in convection duct flow with flapping elastic VG, the present numerical results are compared with theoretical data reported in Ref. [22]. The positive effects of oscillating vortex generation at the different module of elasticity on improving the rate of heat transfer were studied and depicted in Fig. 4. In that figure, the variation of the average Nusselt number with Re on the heated wall is plotted. A good consistency exists between the present findings with those reported by Zheng et al. [22].

6. Results and discussion

The numerical solution and the results for natural convection SAH with elastic VG shown in Fig. 1 are presented and discussed in this section. During the studied cases, both convection flow in ducts with one and two oscillating vortex generators were considered in simulations. In the range of Rayleigh number for the present test cases $(0.5\times10^{10} \le Ra \le 1.5\times10^{10})$, the flow regime is turbulent. All geometrical parameters and also the thermophysical properties used in the mathematical model are reported in Table 1.The values of all geometrical factors for VGs and SAH are chosen in the ranges as they were considered in many similar works [2, 3, 12, 22]. The time history of air velocity is demonstrated in Fig. 5 by plotting the contours of velocity magnitude for turbulent convection flow during the transient time period up to t=10 s, while the system reaches to periodic behavior.

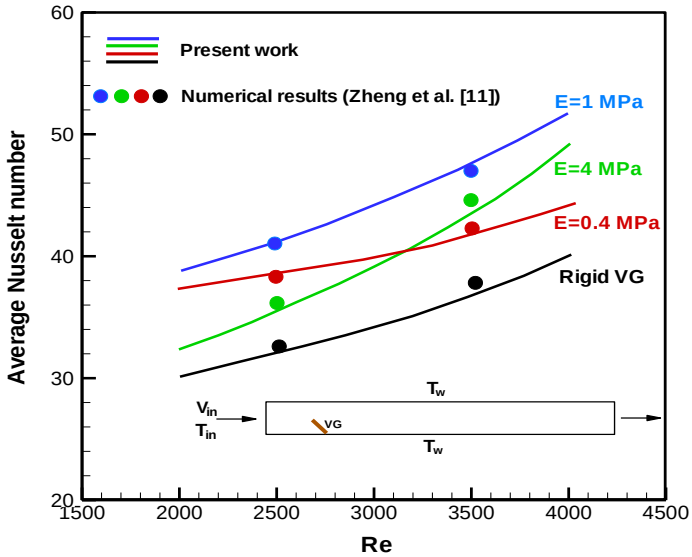

Fig. 4: The variation of average Nusselt number with Re, comparison with theoretical results reported in Ref. [22]

Table 1. Values of parameters for the natural flow SAH

parameter	Value	Parameter	Value
q_{Sun}	$1000\ W/m^2$	T_{amb}	293 K
L	1m	b	8 cm
L_1	0.2 m	L_2	0.3 m
δ	65^0	L_{VG}	33 mm
Δ_{VG}	3 mm	T_{in}	293 K
E	0.01 MPa	ν	0.4

The effects of two vortex generators in the pattern of fluid flow and vortex shedding is clearly observed in Fig. 5. It is seen that the air flows with very low velocity at initial times under the laminar regime and as the air velocity increases with time, the flow breaks down into turbulence. As expected, the air velocity near to the absorber is greater than that is closed to the unheated wall due to the higher buoyancy effect.

Also, Fig.5 depicts that the air velocity increases with time because of the density gradient and after t=10 s while the maximum air flows rate takes place in SAH, a periodic behavior is seen for the velocity field. It is evident that because of the VG oscillation, the system never reaches to steady condition, but a periodic behavior is seen after t=10 s in natural convective flow.

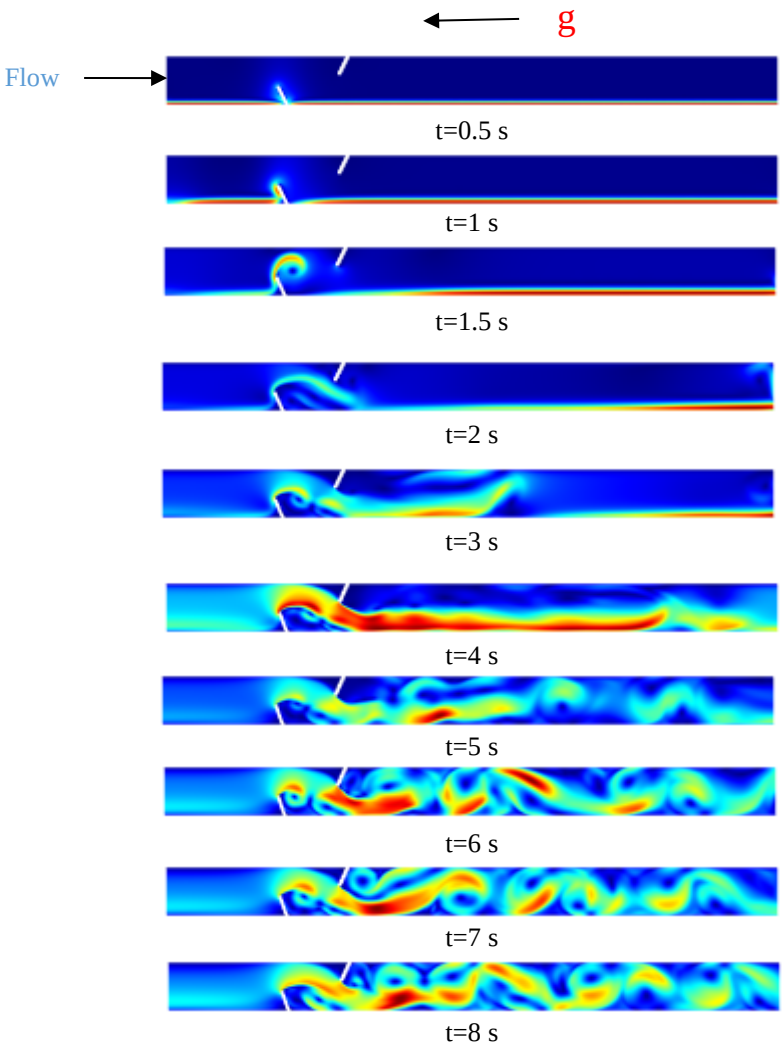

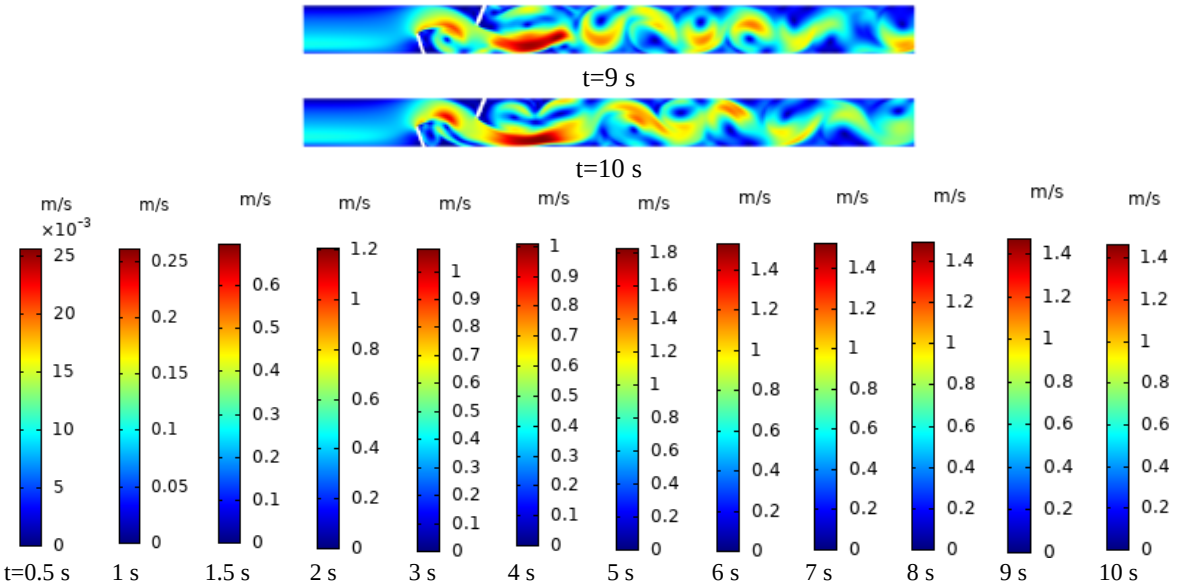

Fig. 5. Contours of velocity magnitude during transient time period up to t=10 s

The time history of air velocity is demonstrated in Fig. 5 by plotting the contours of velocity magnitude for turbulent convection flow during the transient time period up to t=10 s, while the system reaches to periodic behavior. The effects of two vortex generators in the pattern of fluid flow and vortex shedding is clearly observed in Fig. 5. It is seen that the air flows with very low velocity at initial times under the laminar regime and as the air velocity increases with time, the flow breaks down into turbulence. As expected, the air velocity near to the absorber is greater than that is closed to the unheated wall due to the higher buoyancy effect. Also, Fig.5 depicts that the air velocity increases with time because of the density gradient and after t=10 s while the maximum air flows rate takes place in SAH, a periodic behavior is seen for the velocity field. It is evident that because of the VG oscillation, the system never reaches to steady condition, but a periodic behavior is seen after t=10 s in natural convective flow.

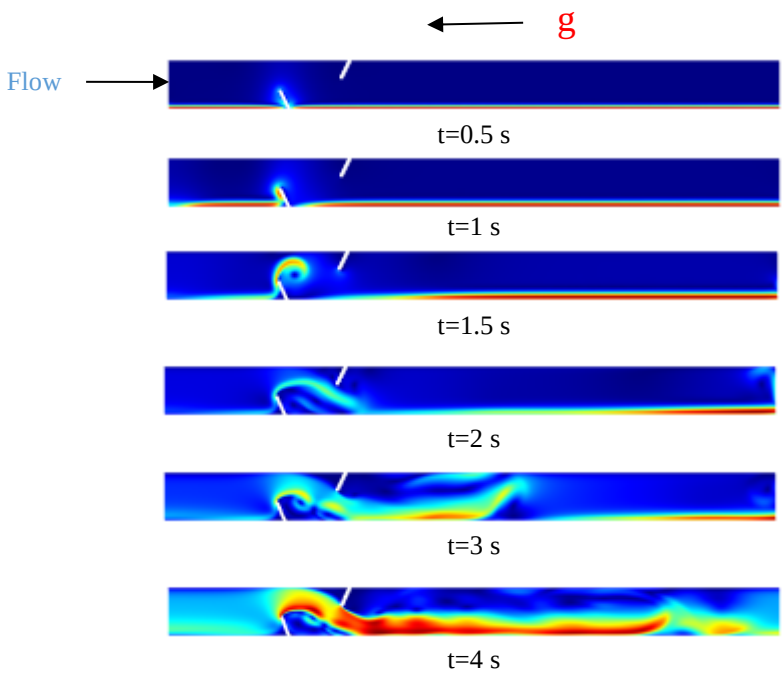

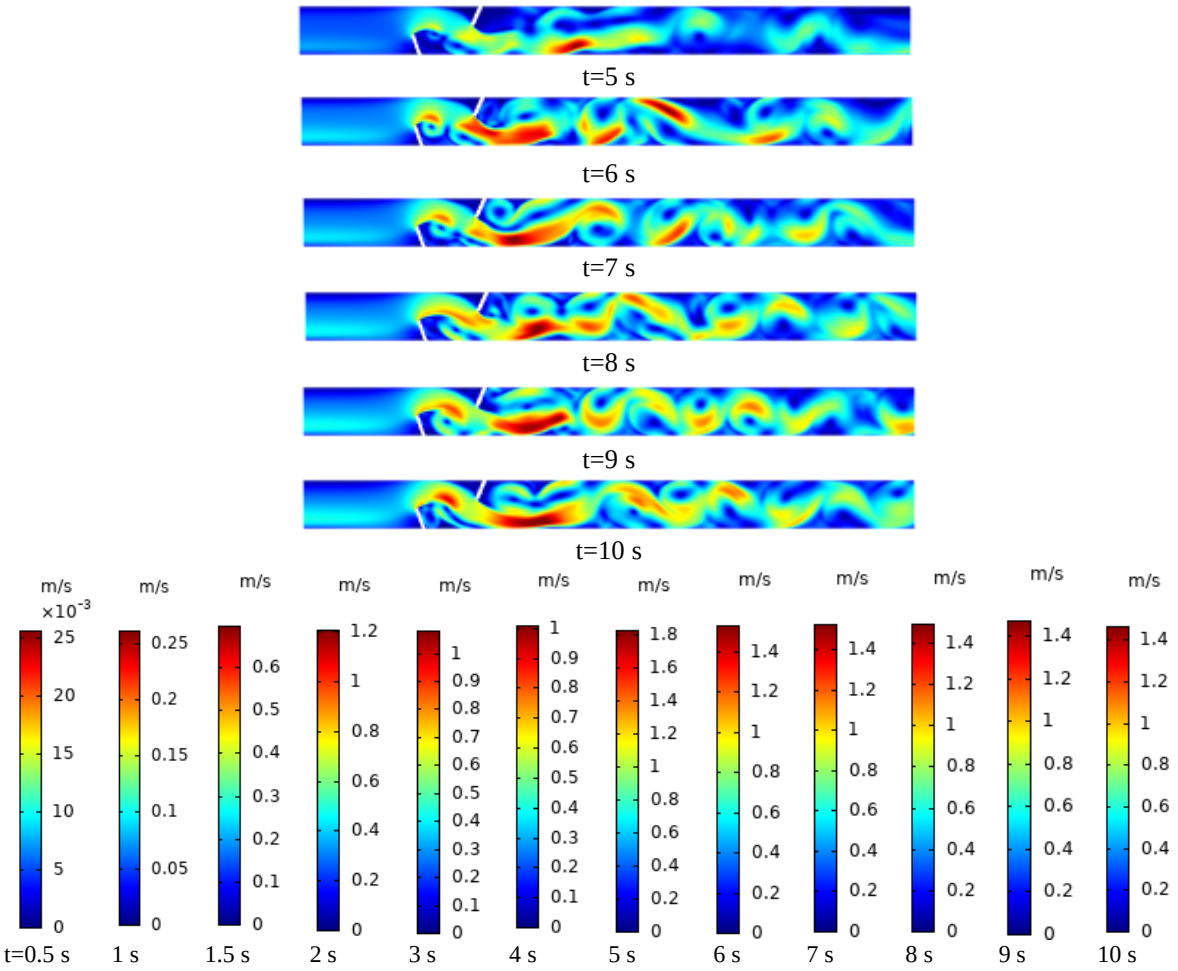

Fig. 5. Contours of velocity magnitude during transient time period up to t=10 s

The temperature contours at different times are plotted in Fig. 6. For all times, there is a hot spot at the intersection point of VG with the heated wall where the fluid remains at a stagnant position. The mixing effect of VGs that leads to breaking the thermal boundary layer adjacent to the absorber and enhancing the convection heat transfer is seen. As it was expected, in the mixing process, the first VG attached to the heated wall is seen as more effective, however, the second one on the other wall is found to be useful after spending the initial time period beyond t=5 s when the airflow has grown enough from the stagnant position. Besides, Fig. 6 demonstrates a transient behavior for the temperature distribution from t=0 s while the air is in a stagnant position up to t=10 s, after which the numerical results reveal a time-periodic pattern for temperature distribution in convective airflow.

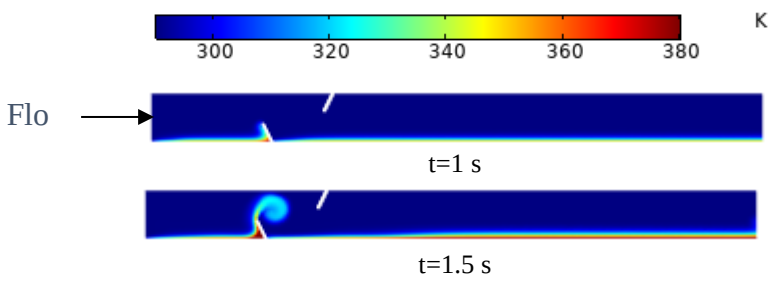

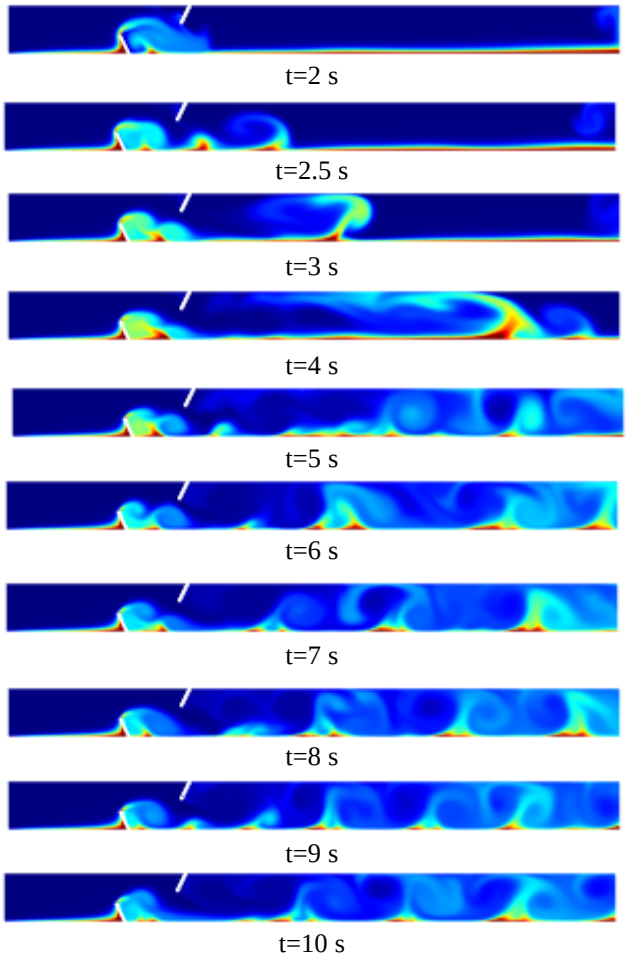

Fig. 6. Temperature contours during transient time period up to t=10 s

The pressure contours at different times are drawn in Fig. 7. The attached point of VG with the heated wall is found as a point with maximum pressure at each time. The moving vortices are also detectable by the low-pressure spots starting from the tip of the two VGs and traveling through the SAH. As it is depicted in Fig. 7, the maximum variation of pressure through the channel is 1.2 Pa which makes this type of flow an isobar one. In contrary to the forced convection in which the fluid pressure gradient plays an important role, the density gradient is the driven body force in free convection. More ever, both ends of SAH are in ambient pressure (zero gauge pressure). The above two factors result in a negligible pressure variation through the buoyant airflow in the natural solar heater.

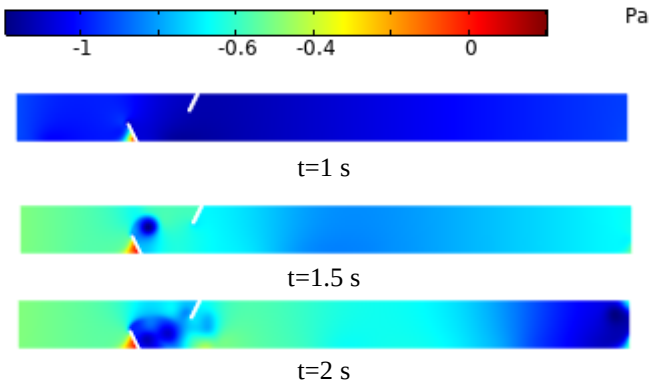

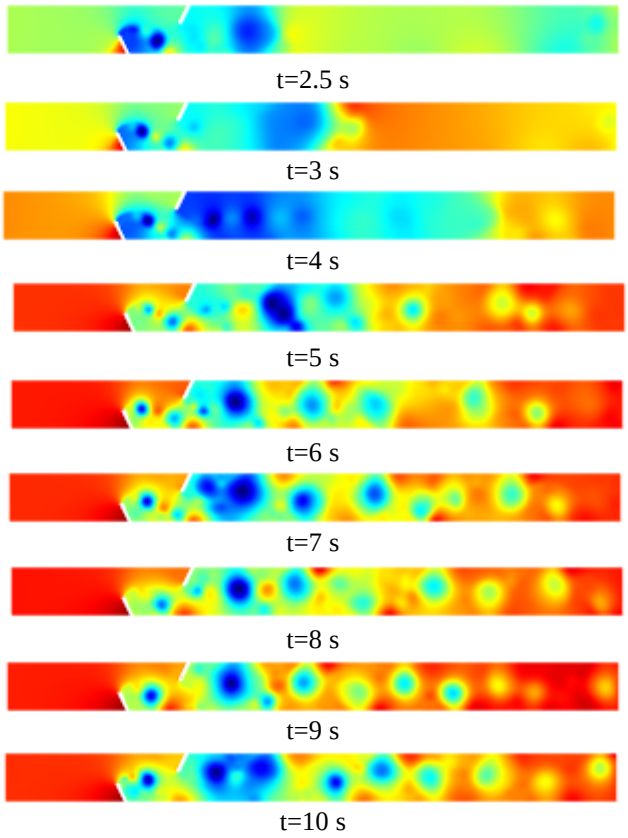

Fig. 7. Pressure contours during transient time period

Similar temperature and velocity contours that were presented for SAH with two vortex generators are also depicted in Figs. 8 and 9 for SAH with single VG. One can compare these figures with those reported before for heaters with double VG to illustrate the positive effect of using two VGs in enhancing heat transfer and improving the thermal performance.

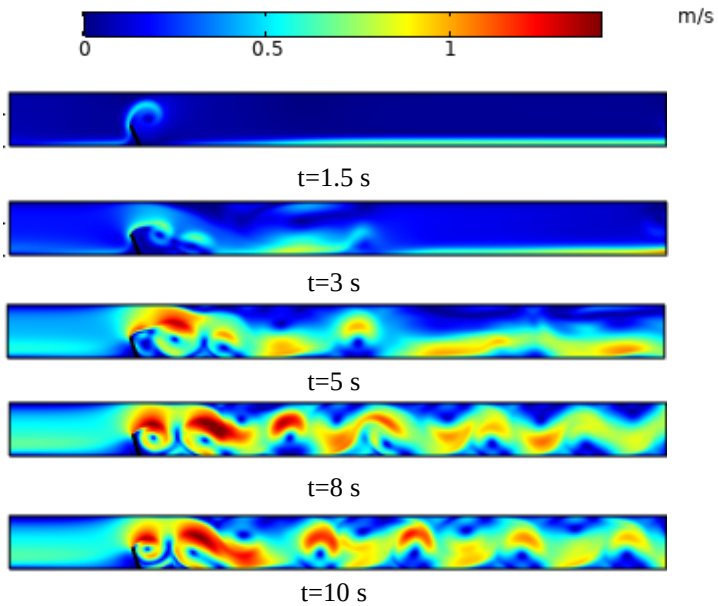

Fig.8. Contours of velocity magnitude during transient time period

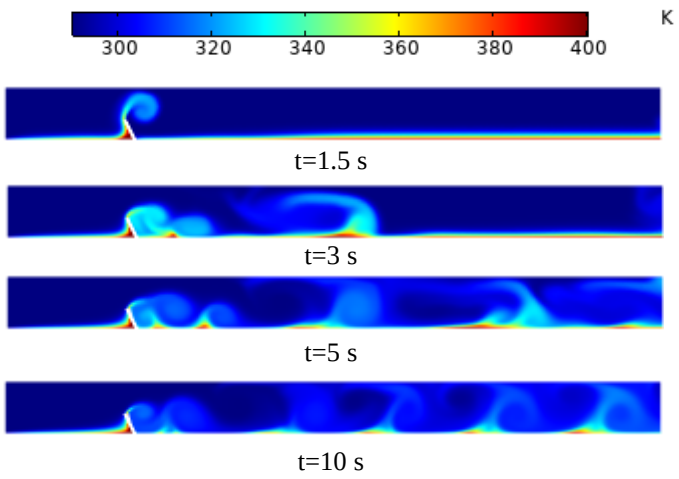

Fig. 9. Temperature contours during the transient time period

In double VG SAH, the displacement variation of the tips of VGs in the x-direction, points A and B, are illustrated in Fig. 10. In the first second of the transient time period, both winglets are stationary although initial airflow was already started on the hot wall. This is due to the blockage effect of the VG that does not allow air at the lower part of VGs to pass and at the same time fluid momentum is not strong enough to bend VG and passes it over. But as the density gradient and buoyant body force increased gradually by receiving more heat from the absorber, airflow started to turn around the VG and passed over it, such that at first, the VG1 oscillates and then VG2 starts its motion (after one second for VG1 and two seconds for VG2). The elasticity of VGs forced to turn their shapes back while the continuous growing momentum of fluid flow resists against them. The VGs actions and airflow reactions lead to transient oscillations of VGs and vortex shedding from the tips which cause fluctuations in the flow field and mixing process. Fig. 10 shows that the VG1 has more displacement than the other winglet because it is near to the heated wall where heat penetration into the airflow takes place and a more buoyant effect exists. However, it is seen that both VGs participate in the vortex generation, vortex shedding and mixing process. For comparison, the displacement of the winglet in a single VG SAH is also depicted in Fig. 10. A similar pattern for oscillation of VG with time is observed with a little more displacement when it compared with the oscillation of the first winglet in double VG SAH.

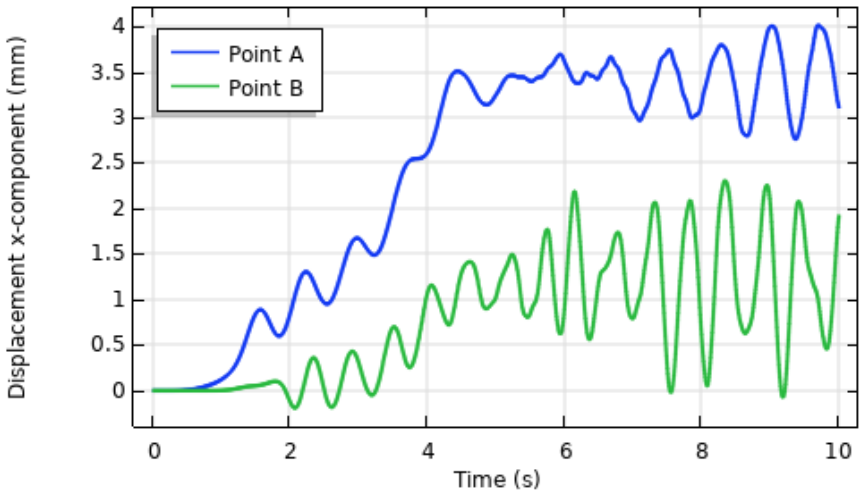

a) Double VG

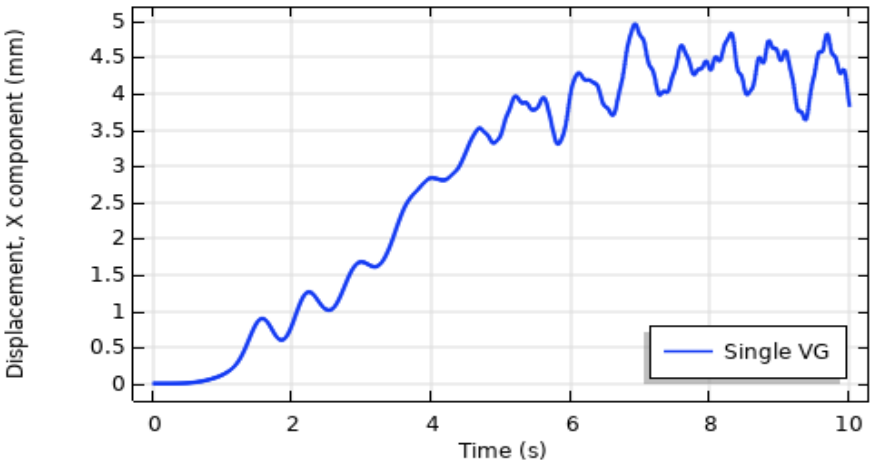

a) Single VG

Fig. 10. Displacements (x-component) of the point(s) on top of VG(s)

The time variations of airflow rates in double and single VG SAHs are plotted in Fig. 11. As expected for two cases, the airflow rate starts from zero value at the initial time and growths during the transient time period, and eventually reaches its maximum value at t=10 s. Moreover, due to the vibration of the vortex generator, variations of both airflow rates are contaminated by fluctuations. Comparison between the flow rates in Fig. 11-a and b reveals that the SAH with double VG has less air flow rate (18%) which is due to a higher blockage effect because of the two winglets, although more mixing rate and vortex generation occurs in this case.

Similar curves but for air bulk temperature at the outlet section are drawn in Fig. 12. At starting time when the airflow has very low velocity, the bulk temperature at the outlet section increases sharply with time, after which it gets a decreasing trend because the airflow rate gets higher value due to buoyancy effect. Moreover, due to the vibration of VG, variations of bulk temperature for both cases were contaminated by considerable fluctuations in the transient time period and also when it gets its periodic oscillation. As the main finding, it should be noted that the air bulk temperature at the outlet section of SAH with double VG is considerably greater than that is for SAH with single VG. If one computes the total rate of heat transfer from the absorber plate into free convection airflow by the relation $q = \dot{m}c_p(T_{m\,out} - T_{in})$ as the main parameter for evaluating the performance of heater, more than 11% increase will be computed for SAH with double VG.

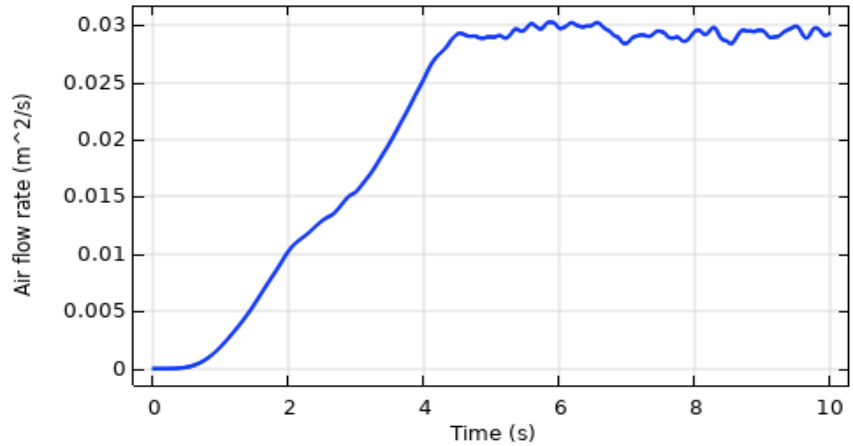

a) SAH with double VG

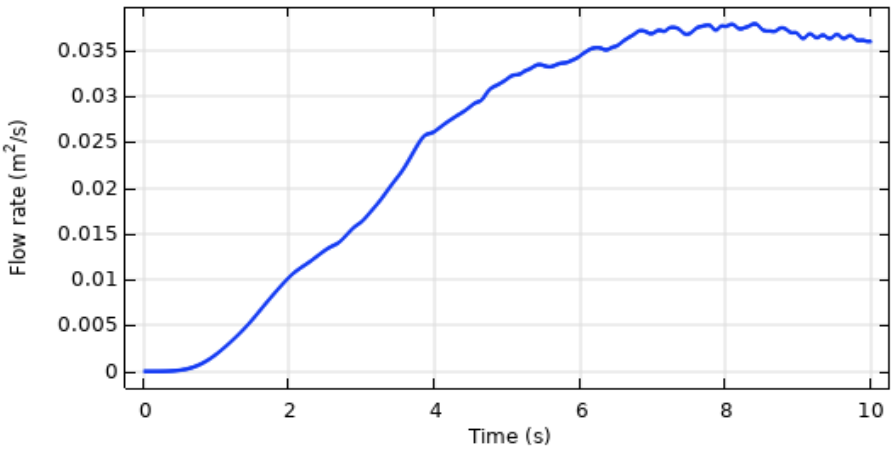

b) SAH with single VG

Fig. 11. Variations of airflow rates with time for single and double VG SAHs

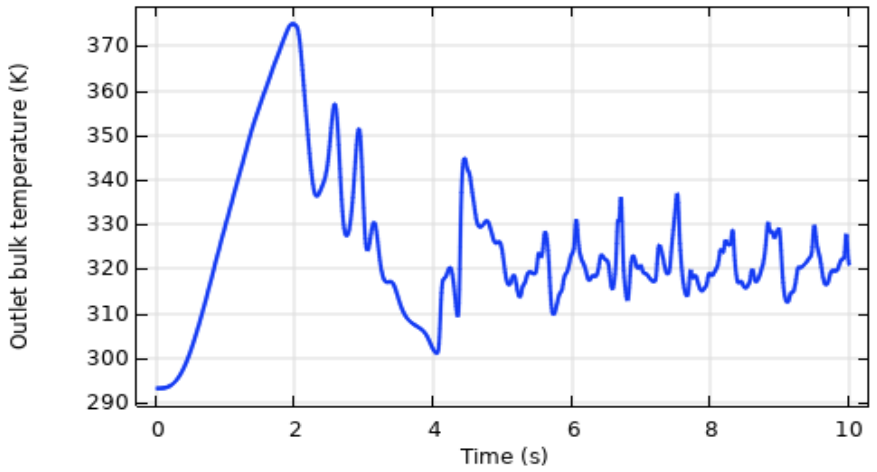

a) Double VG SAH

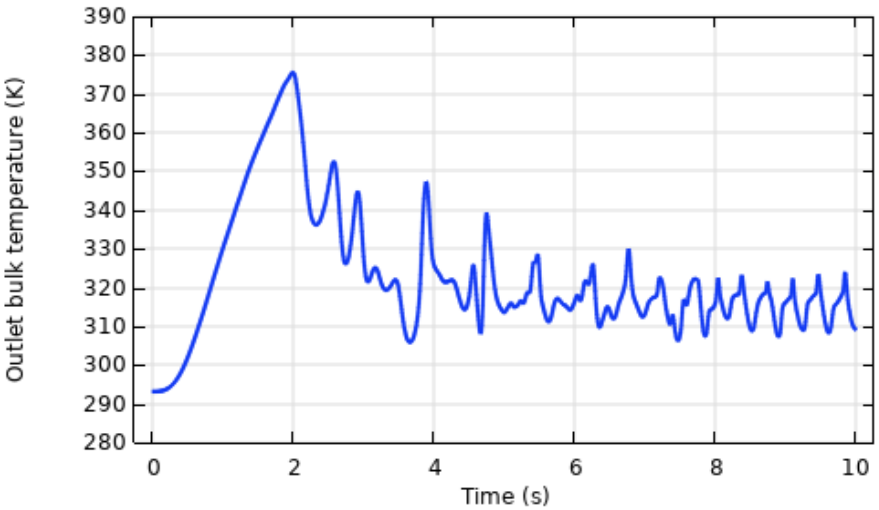

b) Single VG SAH

Fig. 12. Variations of outlet air bulk temperatures with time for SAHs with single and double VG

In order to show the heat transfer enhancement on the heated wall under constant heat flux, it is convenient and usual to show its temperature, as the better heat transfer will cause the lower temperature on the surface because of the high convection coefficient. For this purpose, the absorber temperatures along the x-axis at different times up to t=10 s for two cases are drawn in Fig. 13. As it was noted before, the hot spots on the absorber plate at the intersection of VG is due to blockage and the stagnant airflow behind the winglet. As seen, due to the high mixing rate in SAH with double VG, the absorber temperature for this case is much less than that is for single VG, hence, Fig. 13 confers a better understanding of heat transfer enhancement in the case of double VG SAH.

An attempt was also made to illustrate the flow and thermal behavior of clean SAH for comparing with the heaters with fluctuating winglet. In Fig. 14, the time variations of airflow rate and bulk temperature at the outlet section of clan SAH are plotted. It is seen that although the airflow rate is greater than those were computed for SAH with VG by omitting the winglet blockage effect, the outlet bulk temperature is much less, such that the rate of convective heat transfer from the absorber plate into free convective flow decreases about 29% and 43% in comparison with single and double VG SAHs, respectively.

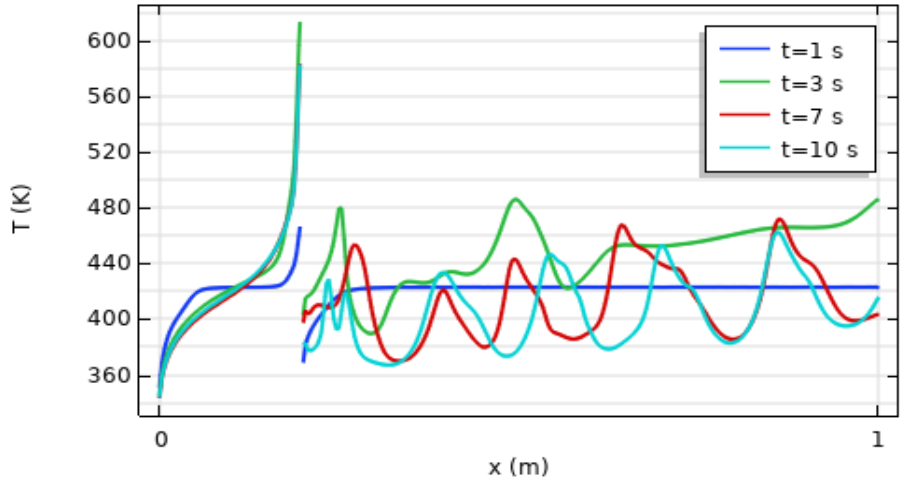

a) Single VG SAH

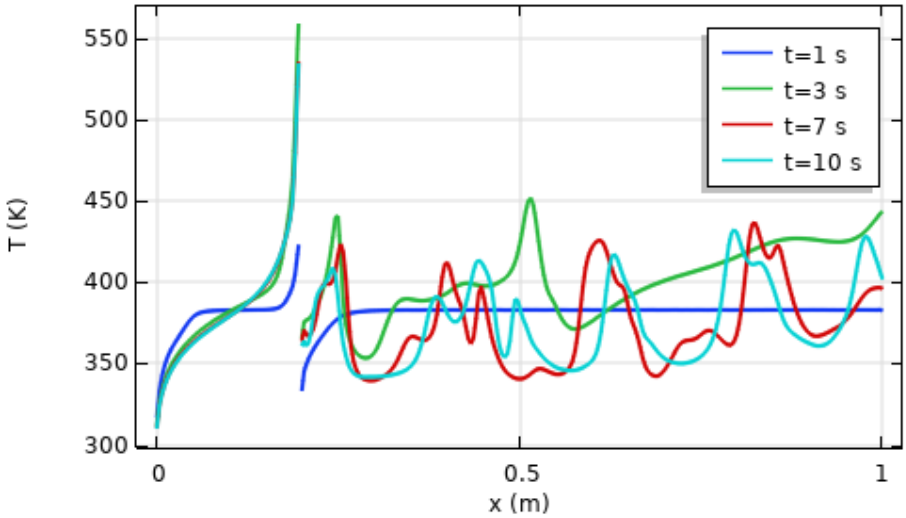

b) Double VG SAH

Fig. 13: Variations of heated wall temperature with time for SAHs

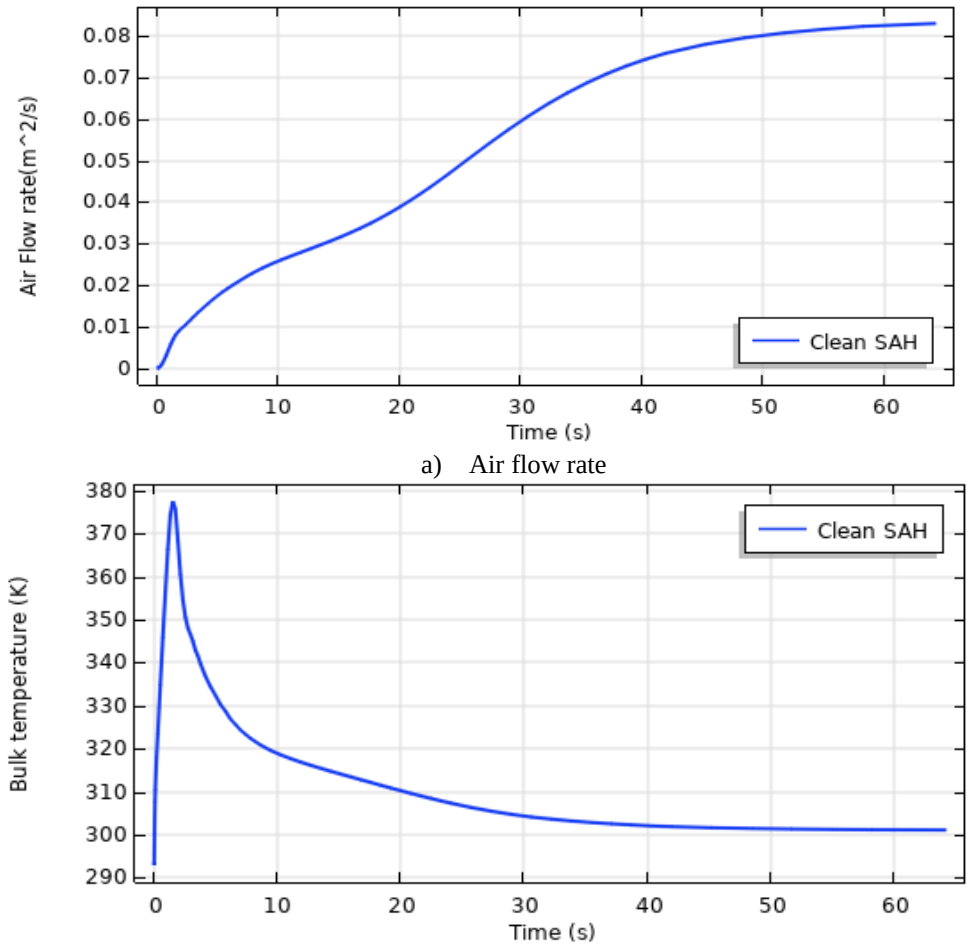

a) Air flow rate

b) Outlet air bulk temperature

Fig. 14: The time variations of airflow rate and bulk temperature at the outlet section of clean SAH

Finally, the velocity distribution under the presence of elastic winglet is compared with the rigid VG in Fig. 15 to demonstrate the positive effect of VG oscillation in generating flow vortices and mixing process in convective airflow through SAH. It should be mentioned that the airflow in a solar heater with a rigid winglet is simulated under steady conditions because the static situation of the VG.

It is seen that because of the vibration of elastic VG against the convective flow, more flow vortices are introduced into the convection flow that causes a higher mixing rate and breaking the thermal boundary layer that finally leads to convection enhancement.

7. Conclusion

Transient 2-D turbulent natural convection heat transfers in solar air heaters with single and double VG were simulated in this paper. The main goal was to compare the performance of

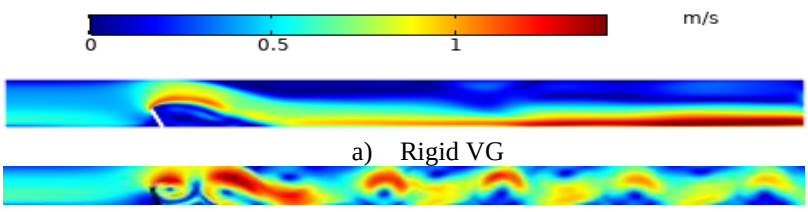

a) Rigid VG

b) Flapping elastic VG (t=10 s)

Fig. 15. Comparison between the velocity fields of air flows in SAHs with rigid and elastic VGs

SAH when one and two flexible winglets are used for having a higher rate of mixing and flow vortices. In the case of double VG SAH, both vortex generators have the same dimensions and attacked angle, as it was considered for single VG SAH. The set of governing equations including the conservation of mass, momentum, and energy for turbulent air convection flow is numerically solved by the FEM. The turbulence modeling is based on the well-known $\kappa-\varepsilon$ model. It was found that the airflow rate in SAH decreases while two VGs are used, which is due to the blockage effect of the winglets against the natural airflow. But temperature computations showed higher air bulk temperature at the outlet section for double VG SAH. Eventually, it was revealed that using two winglets as the vortex generators causes higher performance for SAH in comparison with the single VG SAH, such that for the test cases, about 11% increase in the rate of convection heat transfer from the absorber plate was found. Besides, in comparison with clean SAH, the numerical finding revealed 29% and 43% increase in the rate of convection heat transfer for single and double VG SAHs, respectively. The present numerical results can be used in designing solar-based thermal systems that employ naturally flow solar air heaters as the auxiliary heat source.

References

[1] Hosseini SS, Ramiar A, Ranjbar AA. Numerical investigation of natural convection solar air heater with different fins shape. Renewable Energy 2018: 117: 488–500.

[2] Singh AP, Akshayveer, Kumar A, Singh OP., Designs for high flow natural convection solar air heater, Sol. Energy 2019: 193: 724-737.

[3] Singh AP, Singh OP, Thermo-hydraulic performance enhancement of convex-concave natural convection solar air heaters, Sol. Energy. 2019: 183: 146–161.

[4] Singh S, Experimental and numerical investigations of a single and double pass porous serpentine wavy wiremesh packed bed solar air heater, Renew. Energy. 2020:145: 1361–1387.

[5] Nemś M, Kasperski J, Experimental investigation of concentrated solar air-heater with internal multiple-fin array, Renew. Energy. 2016: 97: 722–730.

[6] Singh S, Performance evaluation of a novel solar air heater with arched absorber plate, Renew. Energy. 2017: 114: 879–886.

[7] Bensaci CE, Moummi A, Sanchez de la Flor FJ, Rodriguez Jara EA, Rincon-Casado A, Ruiz-Pardo A, Numerical and experimental study of the heat transfer and hydraulic performance of solar air heaters with different baffle positions, Renew. Energy. 2020: 155: 1231–1244.

[8] Priyam A, Chand P, Effect of wavelength and amplitude on the performance of wavy finned absorber solar air heater, Renew. Energy. 2018:119: 690–702.

[9] Jin D, Quan S, Zuo J, Xu S, Numerical investigation of heat transfer enhancement in a solar air heater roughened by multiple V-shaped ribs, Renew. Energy. 2019: 134: 78–88.

[10] Sivakandhan C, Arjunan TV, Matheswaran MM, Thermohydraulic performance enhancement of a new hybrid duct solar air heater with inclined rib roughness, Renew. Energy. 2020: 147: 2345–2357.

[11] Singh S, Chaurasiya SK, Negi BS, Chander S, Nemś M, Negi S, Utilizing circular jet enhancement to enhance thermal performance of solar air heater, Renew. Energy. 2020: 154: 1327-1345.

[12] Foruzan Nia M, Gandjalikhan Nassab SA, Ansari AB. Numerical simulation of flow and thermal behavior of radiating gas flow in plane solar heaters, ASME, Journal of thermal sciences and engineering application, 2020: 12: 031008-1.

[13] Dehghani A, Gandjalikhan Nassab SA. Effects of gas radiation on thermal performance of single and double flow plane solar heaters, IJE Transaction C: Aspects 2020: 33(6): 1156-1166

[14] Jacobi AM, Shah RK. Heat transfer surface enhancement through the use of longitudinal vortices, a review of recent progress, Exp. Therm. Fluid Sci. 1995: 11: 295-309.

[15] Leu JS, Wu YH, Jang JY. Heat transfer and fluid flow analysis in plate-fin and tube heat exchangers with a pair of block shape

vortex generators. International Journal of Heat and Mass Transfer 2004: 47: 4327-4338.

[16] Srinil N. Multimode interactions in vortex-induced vibrations of flexible curved/straight structures with geometric nonlinearities. J. Fluid Structure 2010: 26: 1098-1122

[17] Srinil N, Zanganeh H. Modeling of coupled cross flow/in-line vortex-induced vibrations using double Duffering and Van der Pol oscillators. Ocean Eng. 2012: 53(10): 83-97.

[18] Shi J. Hu J. Schafer SR. Chen CL. Numerical study of heat transfer enhancement of channel via vortex-induced vibration. Applied Thermal Engineering 2014: 70: 838- 845.

[19] Ali S. Menanteau S. Habch C. Lemenand T. Harion JL. Heat transfer and mixing enhancement by using multiple freely oscillating flexible vortex generators. Applied Thermal Engineering 2016: 105: 270- 289.

[20] A. K. Soti, R. Bhardwaj, J. Sheridan, Flow-induced deformation of a flexible thin structure as man- ifestation of heat transfer enhancement, International Journal of Heat and Mass Transfer. 2015: 84: 1070-1081.

[21] S. Ali et al., Three-dimensional numerical study of heat transfer and mixing enhancement in a circular pipe using self-sustained oscillating flexible vorticity generators, Chem. Eng. Sci. J. 2017: 162: 152–174.

[22] Zheng L. Xu X. Li K. Chen Y. Huang G. Chen CL. A flapping vortex generator for heat transfer enhancement in a rectangular airside fin. International Journal of Heat and Mass Transfer .2018: 118: 1340- 1356.

[23] Choi SK, Kim SO. Turbulence modeling of natural convection in enclosures: A review, Journal of Mechanical Science and Technology 2012: 26(1): 283-297.

[24] Heindel TJ, Ramadhyani SR, Incropera FP. Assessment of turbulences models for natural convection in enclosure, Numerical Heat Transfer Part B. 1994: 26: 147-172.

[25] Duffie J, Beckman W, Worek M. Solar Engineering Thermal Processes, Second edition 1994: 116.

[26] Cheng X. Müller U. Turbulent natural convection coupled with thermal radiation in large vertical channels with asymmetric heating, Int. J. Heat Mass Transfer. 1998: 41: 1681–1692.